Photon Transport and Hydrodynamics in Gas-Liquid Flows.

Part 1: Characterization of Taylor Flow in a Photo Microreactor.

Anca Roibu, Tom Van Gerven, and Simon Kuhn

Abstract: Gas-liquid photoreactions are increasingly implemented in microreactors. Taylor flows containing an inert dispersed phase were previously used to increase the conversion of photochemical reactions in comparison to using a single liquid phase. However, identifying the optimal flow conditions requires an extensive experimental effort. This work aims to understand the photon transport and hydrodynamics in a Taylor flow photo microreactor so that the reactor behavior can be understood and predicted. Chemical actinometry, flow imaging and residence time distribution experiments were used to develop a multi-region photochemical reaction model. This model shows that the conversion is significantly affected by the liquid distribution, and not by the light scattering or liquid mixing. Moreover, an empirical relation was proposed to predict the optical pathlength in gas-liquid flows. The knowledge gained in this study helps to optimize the performance of Taylor flow photo microreactors, but also to design improved multiphase flow photochemical systems.

Introduction

Gas-liquid photoreactions represent an important segment of photochemical reactions implemented in flow reactors.[1] Most gas-liquid photoreactions are predominantly studied in microreactors due to their small penetration depth and the promotion of segmented flow referred often as slug flow or Taylor flow. This flow pattern consists of an alternation of liquid slugs which are the phase wetting the channel wall (continuous phase), and gas bubbles (dispersed phase) as shown in Figure 1. Between the gas bubbles and the reactor channel wall a thin liquid film is formed. Taylor flow is characterized by an enhanced mixing and interfacial mass transfer and increased safety in comparison to the gas-liquid batch reactor.[2] Among gas-liquid photochemical reactions with a reactive gas phase, the photosensitized addition of singlet oxygen received lately increasing interest and was applied in the synthesis of commercial chemical products as fragrances (e.g. synthesis of fragrance rose oxide from β-citronellol) and pharmaceuticals (e.g. synthesis of the antimalarial artemisinin from dihydroartemisinic acid).[3] Moreover, gas-liquid Taylor flow photoreactors containing an unreactive gas, such as nitrogen, were used to achieve larger conversions compared to using a single liquid phase.[4] The conversion of a photochemical reaction can be increased by using a longer residence time (e.g. by increasing the reactor channel length or reducing the liquid flow rate) and by increasing the intensity of the light source.[5] While these strategies are limited by the properties of the photoreactor and pump, adding an inert phase can be a more accessible option for implementing difficult photochemical processes.[6] Figure 1 illustrates the factors reported to cause this improvement: (i) the presence of a thin liquid film which receives a high photon flux, (ii) light scattering at the interfaces, and (iii) mixing in the liquid slug in two-phase flow.

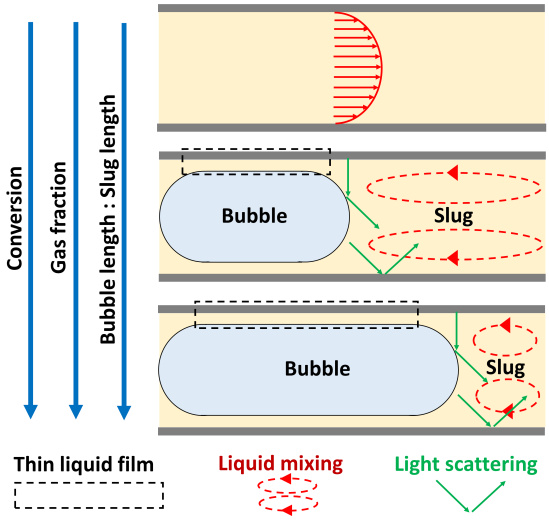

Figure 1. Schematic representation of factors reported to be important in gas-liquid flow with an unreactive gas.

Nakano *et al.* investigated the [2+2] photocycloaddition of carbonyl compounds with olefins, Paternò-Büchi-type photoreactions, in the presence of nitrogen bubbles.[4a] By increasing the gas fraction, the bubble length increased compared to the length of the liquid slug. They found an improvement of the conversion between 40% and 70% in comparison to the single liquid phase when the length ratio between the bubble and slug length was varied between 1:1 to 1:4. A similar increase was found for the product yield. Moreover, they observed that the improvement of the yield in two-phase decreased from around 80% to around 45% when toluene was replaced with trimethyl benzene which is a more viscous solvent. They attributed this observation to the reduction of liquid mixing with increasing viscosity. Previously, they conducted investigations of the same type of reactions in toluene-water Taylor flows.[4b] In this case, toluene was the phase that wetted the channel and water was the unreactive dispersed phase. The observed conversions were discussed in the function of water content. Compared to the photochemical reaction carried out in the single liquid phase, the conversion in two-phase flow was 6.5% higher at a water fraction of 0.2, and reached an increase of 77% at a water fraction of 0.8. An additional study was realized by Nakano *et al.* who analyzed in detail the influence of the light source, concentration, and solvent.[7] Moreover, water was used as the inert phase by Telmesani *et al.* who investigated the photocycloaddition of cinnamates in an ethyl acetate-water Taylor flow.[6] They achieved a conversion of 43% in two-phase flow at a water fraction of 0.9 in comparison to 6% when the water was absent. The addition of water allowed a reduction of the reaction time below 2 hours compared to around 8 hours which was typical for the single-phase reaction. Similar to the previous studies, they observed an increasing conversion with the water fraction which was assigned to the improved mixing due to the long aqueous slugs and short organic slugs. Besides, when the water was replaced by a perfluorinated solvent, the organic slug became the dispersed phase. In this new flow pattern, conversion dropped to 19% compared to 43% when the organic phase was the continuous phase. This experiment proved that the presence of the reagents in the liquid film is crucial.

The studies discussed above showed the potential of the strategy of using an inert immiscible phase and the parameters influencing the conversion. To facilitate the further implementation of this approach, additional knowledge is necessary to predict the optimal reaction conditions without an extensive experimental effort. The characteristics of the flow pattern such as bubbles and slugs length, the film thickness, and the mixing in the liquid slugs are determined by the viscosity and surface tension of the solvent, the wettability of the reactor wall and the flow rates of gas and liquid.[8] While the flow characteristics were previously analyzed in the context of mass transport studies[9], their influence on photon transport was not yet systematically studied.

The light absorption in the photoreactor channel can be experimentally quantified using chemical actinometry. Most of the actinometric measurements realized in microreactors were performed in single phase flow.[5a, 10] While a study was performed in annular flow using the ferrioxalate chemical actinometer[11], the absorption of light in gas-liquid Taylor flow was not previously discussed. Moreover, as the reflection and refraction at the gas-liquid interfaces are difficult to separate from the absorption by experimental means, the influence of scattering can be indirectly analyzed quantifying the optical pathlength. In our previous work, an experimental methodology to simultaneously determine the photon flux and optical pathlength in single liquid phase was described.[12] In comparison to the procedure used for single-phase flow, the chemical actinometry measurements require the experimental determination of the liquid residence time and the volume occupied by the liquid in the reactor. Due to the presence of the thin liquid film formed by the wetting phase, the bubbles travel through a reduced cross-section in comparison to the liquid phase, and as a result the liquid residence time and the liquid volume are sometimes higher than the values calculated using the liquid and gas flow rates.[13]

This study provides understanding how the presence of the gas affects the photoreactions carried out in gas-liquid Taylor flow. This is realized by combining the analysis of photon transport and hydrodynamics in a photo microreactor. Specifically, the bubble and slug lengths and volumes, film thickness, liquid residence time, photon flux per liquid volume and optical pathlength are quantified experimentally at various gas fractions in a photo microreactor. Then, the observed acceleration of the photochemical reaction in two-phase flow is predicted using a multi-zone photochemical reaction model which is developed considering the liquid distribution in the reactor and the photon flux received by the liquid. Moreover, the values of the optical pathlength in two-phase flow are predicted using a function of the gas fraction.

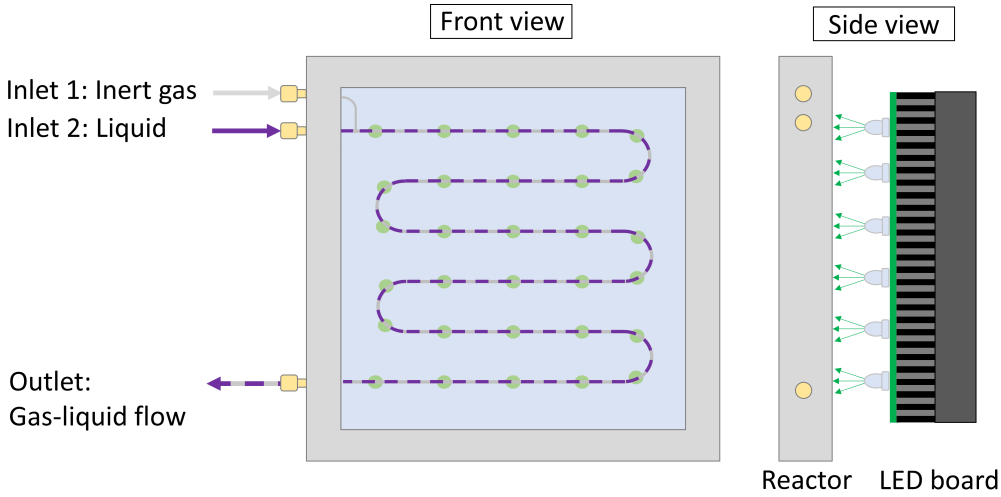

Figure 2. Schematic representation of the photochemical reactor system.

Results and Discussion

Photo microreactor geometry

The photoreactor used in this study is a serpentine channel etched in borosilicate glass. The channel has an internal diameter of 1 mm and a length of 69.9 cm. The plate microreactor is placed at 2 cm from the light source which emits green light. The light source contains 84 LEDs in an arrangement matching the shape of the microchannel (see Figure 2). The current per LED (I_F = 8 mA) was controlled by a driving board. The maximum emission wavelength at this current is around 525 nm. The design and operation of this light source were described in our previous work.[14]

The liquid is introduced into the reactor using a syringe pump and the inert gas, nitrogen, is introduced using a mass flow controller. The gas and liquid streams meet in a T-junction located on the glass plate. Taylor flow was obtained in all the conditions studied in this work. The amount of inert gas introduced into the reactor is discussed in terms of the gas fraction, β_G, which is calculated by dividing the gas flow rate (Q_G) by the sum of gas and liquid flow rates ($Q_G + Q_L$):

$$\beta_G = \frac{Q_G}{Q_L+Q_G} = \frac{Q_G}{Q_{total}} \qquad (1)$$

Influence of gas fraction on actinometer conversion

The photon transport in the gas-liquid Taylor flow was investigated using chemical actinometry. This method involves carrying out a photochemical reaction of which the quantum yield is known. We used the photoizomerization from the closed form to the open form isomer of 1,2-bis(2,4-dimethyl-5-phenyl-3-thienyl)perfluorocyclopentene upon illumination with green light.[12] The quantum yield of this photochemical reaction varies with the irradiation wavelength and is comprised between 0.015 at 480 nm and 0.027 at 620 nm as reported by Sumi et al[15]. By measuring the decrease in the concentration of the closed form diarylethene (DAE CF) after the photochemical reaction, we can back-calculate the photon flux per liquid volume reaching the reagent solution. Previously, we showed that the optical pathlength can be determined in single-phase flow by using a series of chemical actinometer measurements conducted at different starting concentrations of DAE CF and fixed light intensity.[12] This method to determine the optical pathlength becomes even more valuable in gas-liquid phase reactions in comparison to single-phase flow. The heterogeneity of the multiphase flow makes the estimation of the optical pathlength difficult without a ray tracing simulation tool. Consequently, solutions with different starting concentrations of DAE CF in hexane were reacted under green light and analyzed by an online UV-Vis spectrometer at the outlet of the microreactor. The conversions measured in single and two-phase flow are illustrated in Figure 3. The influence of the inert gas on the photochemical reaction was analyzed by performing experiments at different gas fractions while keeping the total flow rate at 1.3 mL min^{-1}.

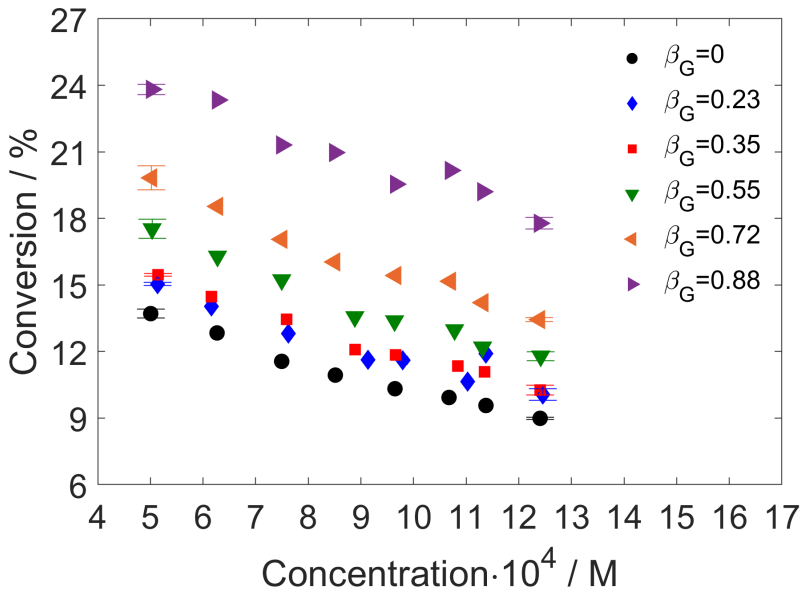

Figure 3. Actinometer conversion in function of starting DAE CF concentration in single-and two-phase flow at various gas fractions, β_G, and the total flow rate of 1.3 mL min^{-1}. Replicates were performed at the highest and lowest starting concentration of DAE CF. The error bars indicate the standard deviations calculated from 3 replicates.

As expected the conversion decreased by increasing the initial DAE CF concentration. The maximum conversion did not exceed 24%. Interestingly, the observed values clearly separate in function of the gas fraction irrespective of the starting concentration of DAE CF. For example, at the highest concentration, we obtained 2-fold higher conversion in two-phase flow at β_G = 0.88 (18%) compared to single-phase flow (9%).

The conversions measured at the starting concentration of 12·10^{-4} M and a total flow rate of 1.3 mL min^{-1} were compared to the conversion values discussed in the introduction. To ease this comparison, the conversions were normalized by the conversion obtained in two-phase flow at the inert phase fraction of β = 0.5. As can be seen in Figure 4, the variation found in our actinometric measurements is similar to the values obtained in the Paternò-Büchi photoreactions by Terao *et al.*[4b] and Nakano *et al.*[7]. However, even if an exponential increase of conversion with the gas content is present also in the work of Telmesani *et al.*[6], the acceleration of the reaction observed by them is significantly higher. This could be due to the different physical properties of their solvent (ethyl acetate vs. toluene and hexane), smaller tube diameter (0.8 mm vs. 1 mm) and different light absorption properties of the employed reaction mixture.

To calculate the photon flux per liquid volume and the optical pathlength from the chemical actinometric measurements we need to determine how long the liquid was illuminated when passing through the microreactor. This was realized using residence time distribution (RTD) experiments.

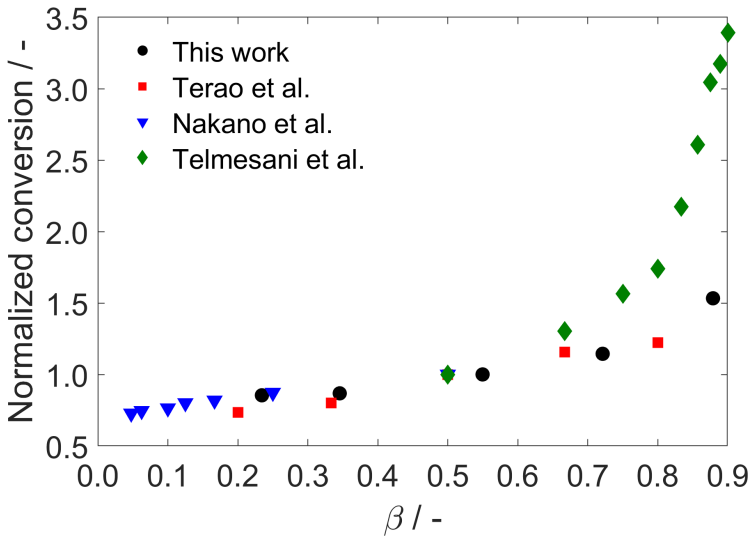

Figure 4. Conversion normalized by the conversion obtained at dispersed phase fraction β = 0.5. The experimental results from this work are compared with the experimental data reported by Terao *et al.*[4b], Nakano *et al.*[7] and Telmesani *et al.*[6]

Liquid residence time in single- and two-phase flow

When assuming that the microreactor behaves like a plug flow reactor, the liquid residence time, $t_{R,calc}$, in single- and two-phase flow can be calculated directly from the reactor volume ($V_{reactor}$) and the total flow rate as follows:

$$t_{R,calc} = \frac{V_{reactor}}{Q_{total}} \quad (2)$$

To verify this assumption, we performed a RTD analysis in liquid and gas-liquid phase. The RTD experiment consists of injecting a tracer solution followed by measuring the variation of its concentration in time at the inlet and outlet of the reactor. The calculation of the experimental liquid residence time, $t_{R,exp}$, from RTD measurements is described in Section S2 in ESI. As can be observed in Table 1, a residence time of 25 s is found for single-phase at 1.3 mL min^{-1} which is close to the calculated value based on the plug flow assumption. The same observation was noticed in two-phase flow for the gas fraction ranged between β_G = 0.23 and β_G = 0.72. However, in the case of the highest gas fraction of β_G = 0.88, the experimental liquid residence time of 28 s was higher than the calculated value of 25 s.

Table 1. Calculated, $t_{R,calc}$, and experimental liquid residence time, $t_{R,exp}$, for single- and two-phase flow at different flow conditions.

Q_{total} mL min^{-1}	β_G -	$t_{R,calc}$ s	$t_{R,exp}$[a] s
1.300	0	25.3	25.4±1.0
1.305	0.23	25.2	24.9±0.4
1.319	0.35	25.0	24.1±0.4
1.305	0.55	25.2	24.8±0.6
1.283	0.72	25.7	25.3±1.4
1.308	0.88	25.2	28.2±1.3

[a] The average and the standard deviation are calculated from 4 replicates.

In this study, the axial dispersion model (ADM) was employed to quantify the axial dispersion in single and two-phase flow. The description of the used methodology is provided in Section S2.4 in ESI. Figure 5 compares the RTD curves found for different gas fractions at 1.3 mL min^{-1}. The broadest distribution was observed for the single-phase flow and two-phase flow at β_G = 0.88. The narrowest distribution was found at the lowest gas fraction of β_G = 0.23.

These observations are in line with previously reported observations.[16] Kreutzer *et al.* correlated the spread of the tracer with the ratio between the slug and bubble lengths which depends on the ratio between the liquid and gas flow rates.[16b] The significant pulse broadening at the highest gas content can be explained by the incomplete mass-exchange between the stagnant long liquid film located around the bubble and the short liquid slugs which allows the tracer to pass into many subsequent slugs.[16b] Therefore, this back-flow could explain the longer liquid residence time of 28 s which was found experimentally at β_G = 0.88. While the broadening is the highest for both the single-phase and the highest gas fraction, these cases had two opposite performances in the photochemical reaction. Therefore, we can conclude that while axial dispersion influences the liquid residence time, the photochemical reaction rate is not affected by it. While this is confirmed for our system, the axial dispersion may have a higher influence on other types of photochemical reactions.

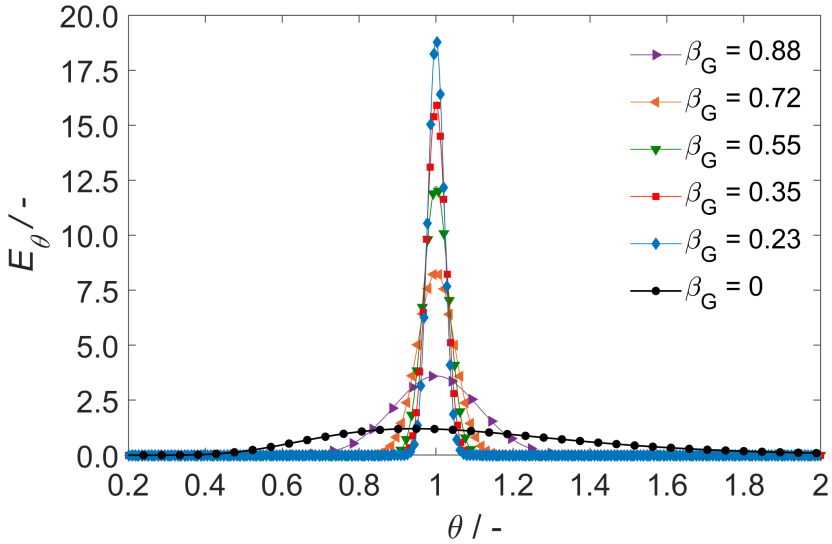

Figure 5. RTD curves obtained from the axial dispersion model (ADM) for single- and two-phase flow at a total flow rate of 1.3 mL min^{-1}.

Photon flux per liquid volume in single- and two-phase flow

The residence times from the RTD study are used to calculate the photon fluxes per liquid volume, I_0^{v}, as follows:[12, 15]

$$I_0^{\mathrm{v}} = \frac{\log\left(10^{\varepsilon_{\mathrm{avg}} c(0) l_{\mathrm{reactor}}} - 1\right) - \log\left(10^{\varepsilon_{\mathrm{avg}} c(t) l_{\mathrm{reactor}}} - 1\right)}{\varepsilon_{\mathrm{avg}} l_{\mathrm{reactor}} \phi_{\mathrm{avg}} t_{\mathrm{R,exp}}} \qquad (3)$$

where $\varepsilon_{\mathrm{avg}}$ is the average molar absorption coefficient (8468 M^{-1} cm^{-1}), $c(0)$ is the initial concentration of DAE CF solution, $c(t)$ is the final concentration of DAE CF solution, l_{reactor} is the average optical pathlength in the liquid, ϕ_{avg} is the average quantum yield (0.021 mol Einstein^{-1}) and $t_{\mathrm{R,exp}}$ is the residence time in the reactor. The values of $\varepsilon_{\mathrm{avg}}$ and ϕ_{avg} are weighted averages between 480 nm and 620 nm and were calculated as described in Section S1.2 in ESI.

As the optical pathlength, l_{reactor}, is unknown, it was fitted together with I_0^{v} using a nonlinear regression model in Matlab (*fitnlm*). It is important to mention that the determination of the two unknowns is possible by assuming that l_{reactor} and I_0^{v} have constant values irrespective of the starting concentration of the chemical actinometer. The obtained photon fluxes per liquid volume, I_0^{v}, are illustrated in Figure 6. As it can be observed, only a limited variation (<5%) of I_0^{v} between the individual data points was found at different concentrations. As the data points are randomly distributed around the average value of I_0^{v}, it is considered that this variation is an experimental error.

Consequently, the methodology developed previously to determine I_0^{v} and l_{reactor} in single-phase flow was successfully applied in two-phase flow and the results are listed in Table 2. I_0^{v} in two-phase flow was divided by its value found in single-phase flow to visualize the improvement of the photoreactor performance by increasing the gas content. The two-phase flow was characterized by up to a 2-fold increase of I_0^{v} at β_G=0.88 compared to the single phase flow. As shown in the previous section, the conversion values differed by the same increase factor of 2 (18% in two-phase flow vs. 9% in single-phase flow).

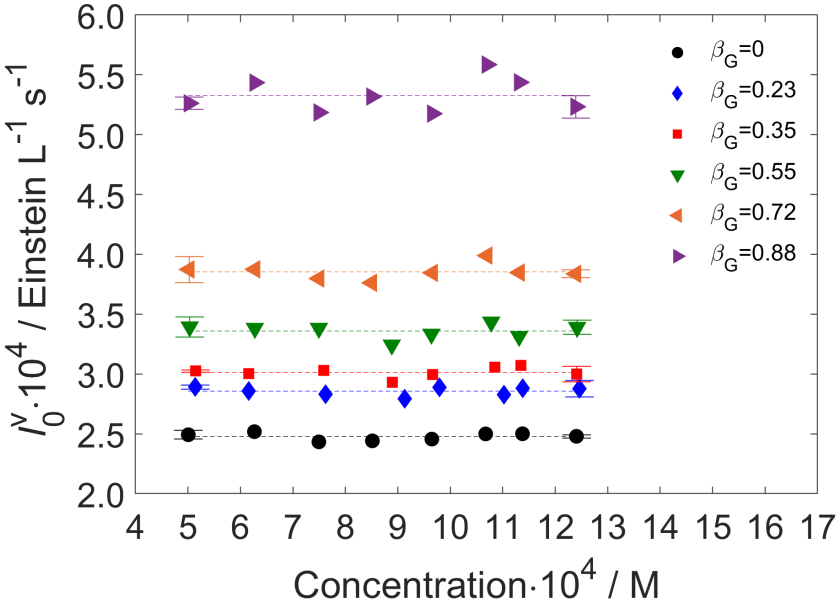

Figure 6. Variation of photon flux per liquid volume, I_0^v, in function of starting actinometer concentration in single- and two-phase flow at a total flow rate of 1.3 mL min^{-1}. The symbols indicate the experimental values and the dotted lines indicate the average values. Replicates were performed at the highest and lowest starting concentration of DAE CF. The error bars indicate the standard deviations calculated from 3 replicates.

Table 2. Photon flux per liquid volume, I_0^v, and optical pathlength, $l_{reactor}$, determined by chemical actinometry at different flow conditions. TP indicates the two-phase flow and SP indicates single-phase flow.

Q_{total} mL min^{-1}	β_G -	$I_0^v \cdot 10^4$ [a] Einstein L^{-1} s^{-1}	$I_{0,TP}^v / I_{0,SP}^v$ -	$l_{reactor}$[a] mm
1.300	0	2.48 ± 0.03	-	0.80 ± 0.02
1.305	0.23	2.86 ± 0.06	1.16	0.77 ± 0.03
1.319	0.35	3.01 ± 0.06	1.22	0.79 ± 0.04
1.305	0.55	3.37 ± 0.08	1.36	0.77 ± 0.04
1.283	0.72	3.85 ± 0.09	1.55	0.75 ± 0.04
1.308	0.88	5.31 ± 0.28	2.14	0.56 ± 0.05

[a] The average and the standard deviation are calculated from all actinometric measurements acquired at the indicated flow conditions.

Moreover, Table 2 presents the values of the optical pathlength found in single-phase and two-phase flow. The determined optical pathlengths represent the average distances that photons travel and are absorbed in different liquid regions of the two-phase flow. By increasing the gas fraction between β_G = 0 to β_G = 0.88, the optical pathlength decreased from 0.80 mm to 0.56 mm. This large decrease of the optical pathlength at β_G = 0.88, indicates that the reaction took place predominantly in the liquid film and less in the liquid slug. For the first time, we were able to experimentally quantify the influence of the gas bubbles on the optical pathlength in Taylor flow.

Investigation of mass transfer limitations

Taylor flow is characterized by a liquid recirculation which improves the radial mixing in comparison to single-phase flow. The mixing in the liquid slugs could be correlated to the number of revolutions in the slug or the recirculation rate.[17] We investigated the influence of the recirculation rate by performing chemical actinometric measurements at the same gas fraction of β_G = 0.55 and two additional total flow rates of 0.56 mL min^{-1} and 0.82 mL

min^{-1} (see Figure S1.6 in ESI). As can be seen in Table 3, similar photon flux per liquid volume and optical pathlengths were obtained irrespective of the flow rate. This indicates that the photoreactions performed in this study were not limited by the recirculation rate in the liquid slug.

Table 3. Comparison of photon flux per liquid volume, I_0^v, and optical pathlength, $l_{reactor}$, determined by chemical actinometry at a fixed gas fraction, β_G, and different total flow rates, Q_{total}.

Q_{total} mL min^{-1}	β_G -	$I_0^v \cdot 10^4$ [a] Einstein L^{-1} s^{-1}	$l_{reactor}$[a] mm
1.305	0.55	3.37 ± 0.08	0.77 ± 0.04
0.823	0.55	3.38 ± 0.09	0.79 ± 0.04
0.557	0.55	3.39 ± 0.07	0.81 ± 0.04

[a] The average and the standard deviation are calculated from all actinometric measurements acquired at the indicated flow conditions.

Moreover, to further check if the conducted photochemical reactions were photon or mass transport limited, we performed them at different light intensities. The intensity of the light source is directly proportional to the current through the LEDs.[14] Therefore, we compared the photoreactor performance at 4 mA/LED and 8 mA/LED. In case the photochemical reaction is mass transfer limited in single-phase, but not in two-phase flow at β_G = 0.88, I_0^v should change with a different factor. As can be seen in Table 4, I_0^v is twice the value at 8 mA/LED obtained at both single- and two-phase flow at β_G = 0.88. Due to the similar ratio of $I_{0,8mA}^v/I_{0,4mA}^v$ and the lack of influence of the rate of recirculation on the chemical actinometry results we conclude that the photochemical reaction is in the photon-limited regime in both single- and two-phase flow. Consequently, the liquid mixing was excluded to be a source for increasing the conversion in two-phase flow in our study. However, the presence of mass transfer limitations is specific to each individual photochemical reaction and experimental conditions and needs to be verified accordingly.

Table 4. Comparison of photon flux per liquid volume, I_0^v, and optical pathlength, $l_{reactor}$, determined by chemical actinometry at 4 mA/LED and 8 mA/LED.

Current/LED mA	Q_{total} mL min^{-1}	β_G -	$I_0^v \cdot 10^4$ [a] Einstein L^{-1} s^{-1}		$I_{0,8mA}^v/I_{0,4mA}^v$ -
4	1	0	1.34	± 0.05	2.0
8	1	0	2.68	± 0.06	
4	1.308	0.88	2.79	± 0.13	1.9
8	1.308	0.88	5.31	± 0.28	

[a] The average and the standard deviation are calculated from all actinometric measurements acquired at the indicated flow conditions.

Characterization of the gas-liquid flow pattern

As discussed in the introduction, the slug and bubble lengths, and the presence of the liquid film located around the bubble have an important influence on the performance of the photoreactor. Therefore, these flow characteristics were measured in this study by flow imaging. Figure 7 illustrates a Taylor flow pattern in a microchannel characterized by a cross-section area, A. We considered that the length of a bubble, L_b, is the distance between the nose and the rear of the same bubble, and the slug length, L_s, is the distance between the

rear and nose of two consecutive gas bubbles. Moreover, it is assumed that a wetting liquid film with a constant thickness, δ_f, is formed on the channel wall and surrounds both the gas bubbles and liquid slugs.[18] This liquid film is assumed stagnant and hence the bubble travels through a reduced cross-section area, A_b. As will be shown below, these assumptions allow us to calculate the film thickness from the bubble velocity.

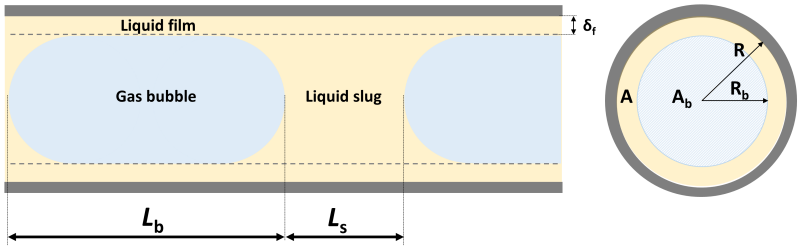

Figure 7. Schematic representation of gas-liquid Taylor flow in a microreactor (not to scale).

Figure 8 illustrates the flow patterns obtained at gas fractions β_G = 0.23-0.88 at 1.3 mL min^{-1} and different total flow rates of 0.56 mL min^{-1}, 0.82 mL min^{-1} and 1.3 mL min^{-1} at β_G = 0.55. As observed, the nose and the rear of the bubbles can be approximated as hemispherical caps in all investigated conditions. The procedure to measure the bubble and the slug lengths is presented in Section S3.1 in ESI, and the resulting values are shown in Figure 9. The lowest and the highest gas fractions were characterized by a higher instability of the gas-liquid flow in comparison to other conditions which translated in a larger standard deviation for the average bubble and slug lengths. These variations of bubble and slug length could be caused by the pulsation of the syringe pump, pressure fluctuations due to the bubble formation and leaving the channel[19] or a non-uniform diameter of the channel. By increasing the gas fraction from β_G = 0.23 to 0.88 at 1.3 mL min^{-1}, the slug length strictly decreased from 5 mm to 1.4 mm, while the bubble length strictly increased from 1.9 mm to 12.8 mm. While these values cannot be compared directly as the sum L_b+L_s is not constant, the different flow patterns can be analyzed in terms of the length ratio L_b/L_s. As can be observed in Table 5, L_b/L_s increased with the gas fraction. Therefore, the higher L_b/L_s the larger was the I_0^V (see Table 2) and the conversion (see Figure 3).

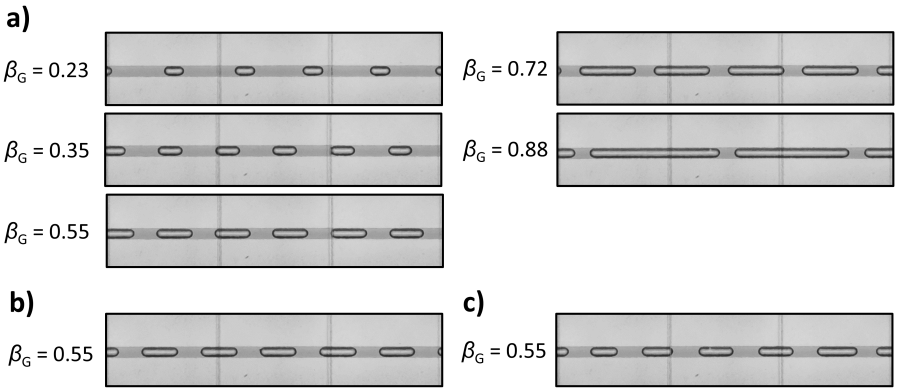

Figure 8. Images of the resulting gas-liquid flow pattern at various gas fractions, β_G, and total flow rates of a) 1.3 mL min^{-1}, b) 0.82 mL min^{-1} and c) 0.56 mL min^{-1}.

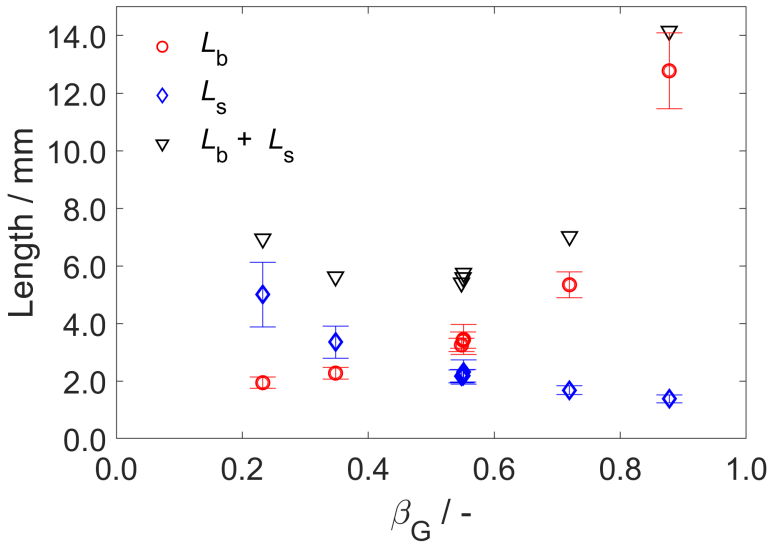

Figure 9. Comparison of average bubble length, L_b, slug length, L_s, and their sum, L_b+L_s, at various gas fractions, β_G, and a total flow rate of 1.3 mL min^{-1}. In addition, the lengths at β_G = 0.55 and total flow rates of 0.82 mL min^{-1} and 0.56 mL min^{-1} are illustrated. The standard deviations of the average bubble and slug lengths are illustrated by error bars.

Table 5. Characteristics of studied gas-liquid flow pattern determined using flow imaging.

Q_{total}	β_G	L_b/L_s	u_b[a]	A/A_b	δ_f
mL min^{-1}	-	-	cm s^{-1}	-	μm
1.303	0.233	0.39	3.17 ± 0.02	1.15	33.3
1.319	0.348	0.68	3.26 ± 0.05	1.16	36.7
1.305	0.548	1.51	3.20 ± 0.04	1.15	34.6
1.283	0.719	3.18	3.14 ± 0.06	1.15	34.3
1.308	0.878	9.26	3.24 ± 0.04	1.17	37.4
0.823	0.550	1.57	2.05 ± 0.03	1.17	38.7
0.557	0.551	1.49	1.39 ± 0.04	1.18	38.8

[a] The average and the standard deviation for the bubble velocity calculated from the analysis of 5 bubbles.

Moreover, by comparing the flow pattern at β_G = 0.55 and total flow rates of 0.56, 0.82 and 1.3 mL min^{-1}, it can be concluded that the total flow rate did not significantly affect the bubble and slug lengths. These constant bubble and slug lengths explain why similar results in the chemical actinometric measurements were observed at β_G = 0.55 irrespective of the total flow rate.

The next investigated aspect was the bubble velocity, u_b. The two-phase flow superficial velocity, U_{total}, was calculated as:

$$U_{\text{total}} = \frac{Q_{\text{total}}}{A} \quad (4)$$

In reality, the bubble travels faster than U_{total} due to the presence of the stagnant film. From continuity, the bubble velocity, u_b, will be larger than the total velocity in the channel, U_{total}, by a factor of A/A_b:

$$u_{\text{b}} = \frac{A}{A_{\text{b}}} U_{\text{total}} \quad (5)$$

The velocity of the bubble was experimentally determined using recorded videos of the two-phase flow (see Section S3.2 in ESI). As can be seen in Table 5, the measured bubble velocity was 1.15-1.18 higher than the two-phase velocity. Then, the cross-sectional area A_b can be easily determined from the experimental value of the ratio A/A_b.

A_b was further used to calculate the liquid film thickness as follows:

$$\delta_f = R - R_b = \sqrt{\frac{A}{\pi}} - \sqrt{\frac{A_b}{\pi}} \quad (6)$$

where R is the radius of the reactor channel and R_b is the radius of the gas bubble.
As can be seen in Table 5, the determined film thickness was around 35 µm and was almost constant across all investigated conditions. This is surprising because it exceeds the values between 2.5 µm (at 0.56 mL min^{-1}) and 5.5 µm (at 1.3 mL min^{-1}) predicted using Bretherton's correlation[20]:

$$\frac{\delta_f}{d} = 0.66\mathrm{Ca}^{2/3} \quad (7)$$

where d is the diameter of the channel and Ca is the Capillary number. The thicker liquid film found in our microreactor can be caused by several factors: (i) The presence of the organic compound which changes the physical properties of hexane. (ii) The presence of surfactant traces (Marangoni effects).[21] (iii) The roughness of the channel which leads to a constant value of film thickness which does not vary with the bubble velocity.[22]

Prediction of the photon flux per liquid volume

In this work, a large ratio of L_b/L_s is correlated to a large I_0^v and consequently improved conversion. This was correlated to the longer liquid film located around the gas bubble obtained at large L_b/L_s. However, this length ratio does not capture the influence of the film thickness. Therefore, we propose to divide the reactor space in reaction zones characterized by a specific I_0^v and liquid volume. Figure 10 compares the different reaction regions defined for single- and two-phase flow. The single-phase flow consists of a region of a continuous liquid film with the volume of V_{film} and a region of bulk liquid with the volume of V_{bulk}. The film zone is defined based on the film thickness experimentally determined in two-phase flow.

The two-phase flow consists of three regions, due to the additional liquid present around the bubble caps. This zone is characterized by the liquid volume of V_{caps}. While Figure 10 illustrates only a unit cell (one gas bubble and one liquid slug), these volumes V_{film}, V_{bulk}, and V_{caps} represent the total volume in the reactor distributed in the liquid film, in the bulk liquid, and around the bubble caps.

It is assumed that no photoreaction takes place in the gas bubble, the actinometric measurements are carried out in the absence of mass transfer limitations and the light scattering does not have a significant effect on the photoreactor performance. Next, a simple model is developed based on the photon flux per liquid volume and the liquid volume specific to each reaction zone.

The photon flux $I_0^v V_{liquid}$ determined using chemical actinometry represents the sum of the photon flux received in the liquid film $I_{0,film}^v V_{film}$, in the liquid bulk $I_{0,bulk}^v V_{bulk}$ and in the liquid around the bubble caps, $I_{0,caps}^v V_{caps}$ (only for the two-phase flow) as follows:

$$I_0^v V_{liquid} = I_{0,bulk}^v V_{bulk} + I_{0,film}^v V_{film} + I_{0,caps}^v V_{caps} \quad (8)$$

By summing the liquid volume present in the film, bulk and around the bubble caps, the total liquid volume present at a certain time in the reactor can be calculated.

$$V_{liquid} = V_{film} + V_{bulk} + V_{caps} \quad (9)$$

The calculation of V_{liquid}, V_{bulk}, and V_{film} is detailed in Section S3.3 in ESI. It is important to mention that when the total liquid volume in the reactor, V_{liquid}, was estimated using the gas fraction, β_G, the volume was underestimated for all flow conditions.

$$V_{liquid} \neq (1 - \beta_G)\, V_{reactor} \quad (10)$$

Therefore, the value of V_{liquid} used in this model was determined experimentally using flow imaging and illustrated in Figure 11. As the gas fraction is increased, the volume of the bubble increases and V_{liquid} decreases linearly from 0.55 mL at β_G = 0 down to 0.14 mL at β_G = 0.88. This decrease is due to the drop of V_{bulk}, as V_{film} and V_{caps} are almost constant at 0.08 mL and 0.02 mL, respectively.

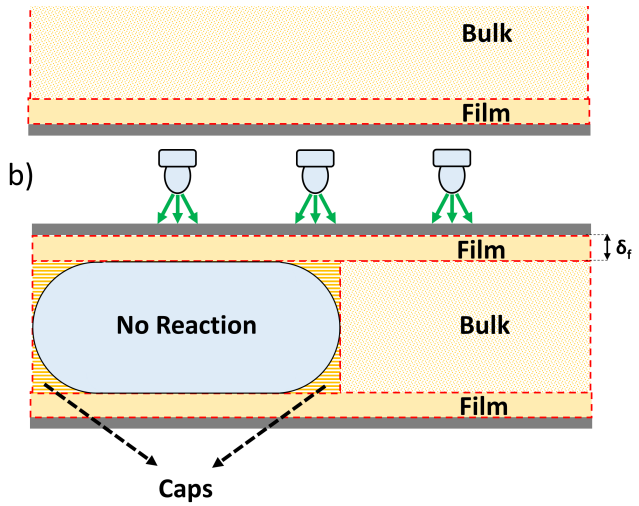

Figure 10. Schematic representation of the reaction zones considered in the model. a) Liquid zones in the single-phase flow: liquid film and liquid bulk. b) Liquid zones in the two-phase flow: liquid film, liquid bulk and the liquid around the bubble caps.

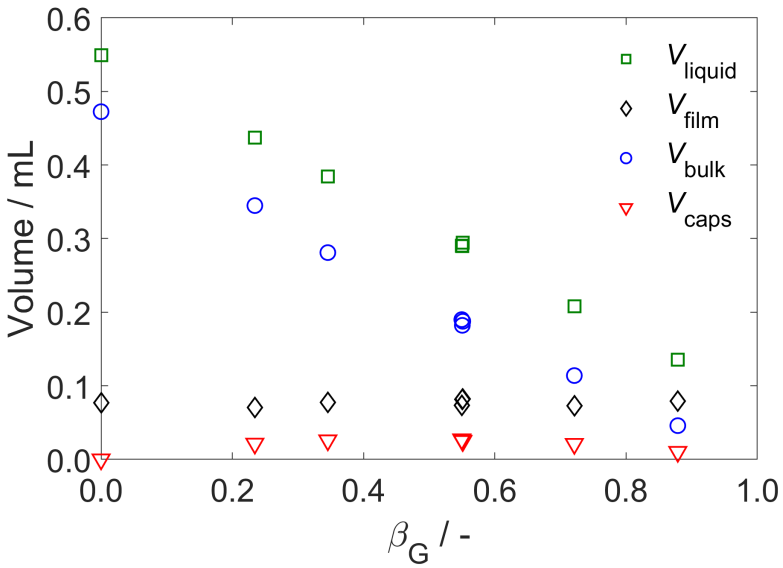

Figure 11. Variation of the liquid volume in the reactor, V_{liquid}, in the film, V_{film}, in the bulk, V_{bulk}, and around the bubble caps, V_{caps}, in function of the gas fraction, β_G, at a total flow rate of 1.3 mL min^{-1}. In addition, the liquid volumes are shown for β_G = 0.55 at total flow rates of 0.82 mL min^{-1} and 0.56 mL min^{-1}.

Therefore, the photon flux per liquid volume in the liquid bulk, $I^{v}_{0,bulk}$, can be determined from the slope of the curve $I^{v}_{0} V_{liquid}$ vs. V_{bulk} as indicated in equation (11) and Figure 12.

$$\underbrace{I^{v}_{0} V_{liquid}}_{y} = \underbrace{I^{v}_{0,bulk}}_{slope} \underbrace{V_{bulk}}_{x} + \underbrace{I^{v}_{0,film} V_{film} + I^{v}_{0,caps} V_{caps}}_{intercept} \qquad (11)$$

It was found that $I^{v}_{0,bulk}$ is equal to 1.87·10^{-4} Einstein L^{-1}s^{-1}. Next, the value corresponding to the film region $I^{v}_{0,film}$ can be calculated from the equation (11) applied to single-phase flow (V_{caps} = 0).

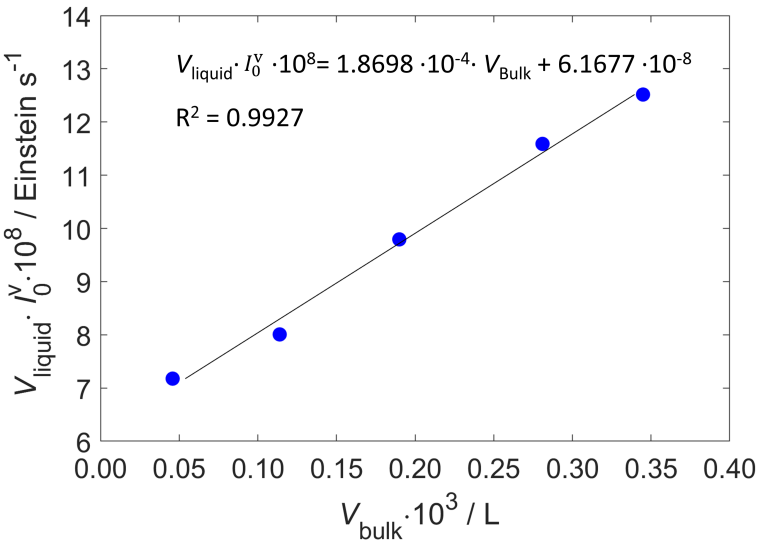

Figure 12. Determination of the regional photon fluxes per liquid volume from slope and intercept of the linear regression at a total flow rate of 1.3 mL min^{-1}.

$$I_{0,\mathrm{film}}^{\mathrm{v}} = \frac{V_{\mathrm{liquid}} I_0^{\mathrm{v}} - V_{\mathrm{bulk}} I_{0,\mathrm{bulk}}^{\mathrm{v}}}{V_{\mathrm{film}}} \qquad (12)$$

It is found that $I_{0,\mathrm{film}}^{\mathrm{v}}$is equal to 6.23·10^{-4} Einstein L^{-1}s^{-1}. Finally, $I_{0,\mathrm{caps}}^{\mathrm{v}}$ was calculated from the intercept and $I_{0,\mathrm{film}}^{\mathrm{v}}$ as follows:

$$I_{0,\mathrm{caps}}^{\mathrm{v}} = \frac{\mathrm{intercept} - V_{\mathrm{film}} I_{0,\mathrm{film}}^{\mathrm{v}}}{V_{\mathrm{caps}}} \qquad (13)$$

The value of $I_{0,\mathrm{caps}}^{\mathrm{v}}$ was found to be equal to 6.19·10^{-4} Einstein L^{-1}s^{-1}.

When comparing the results of the model summarized in Table 6, it can be observed that the liquid film zone is characterized by only a slightly higher photon flux per liquid volume than the region around the bubble caps, but it is 3.3 times higher in comparison to the liquid slug. While this variation could be explained by (i) the photon flux gradient across the channel due to light absorption, or (ii) the gradient in velocity due to the Poiseuille velocity profile, we propose that light attenuation is the most probable cause.

Table 6. Regional photon flux per liquid volume, $I_{0,\mathrm{film}}^{\mathrm{v}}$, $I_{0,\mathrm{bulk}}^{\mathrm{v}}$ and $I_{0,\mathrm{caps}}^{\mathrm{v}}$ determined with the multi-zone photochemical reaction model.

$I_{0,\mathrm{film}}^{\mathrm{v}} \cdot 10^4$	$I_{0,\mathrm{bulk}}^{\mathrm{v}} \cdot 10^4$	$I_{0,\mathrm{caps}}^{\mathrm{v}} \cdot 10^4$
Einstein L^{-1}s^{-1}	Einstein L^{-1}s^{-1}	Einstein L^{-1}s^{-1}
6.23	1.87	6.19

The obtained values of $I_{0,\mathrm{bulk}}^{\mathrm{v}}$, $I_{0,\mathrm{film}}^{\mathrm{v}}$ and $I_{0,\mathrm{caps}}^{\mathrm{v}}$ are used in equation (11) to predict the overall photon flux per liquid volume. As shown in Figure 13, a good match was found between the predicted and experimental values. This observation applied also for the data points determined at lower flow rates, 0.82 mL min^{-1} and 0.56 mL min^{-1}, which were not used in the fitting.

This model was developed to explain and predict the increase of I_0^{v} with the gas content observed in our study. However, the application of the model could be extended to guide the optimization of two-phase photochemical reactions. By comparing the absolute photon flux values for each flow condition to the single-phase value (see Table S3 in ESI), we observe that the two-phase flow is characterized by a higher photon loss. When an inert gas phase is introduced in the reactor, a part of the photons which otherwise would be absorbed by the liquid are lost in the surrounding environment.

Moreover, a lower productivity is expected in two-phase flow as a fraction of the reactor is occupied by the inert phase. However, higher productivities in two-phase flow compared to single-phase were achieved by using a very low fraction of the inert phase (Nakano et *al.*[7]) or by using highly concentrated solutions (Telmesani et *al.*[6]).

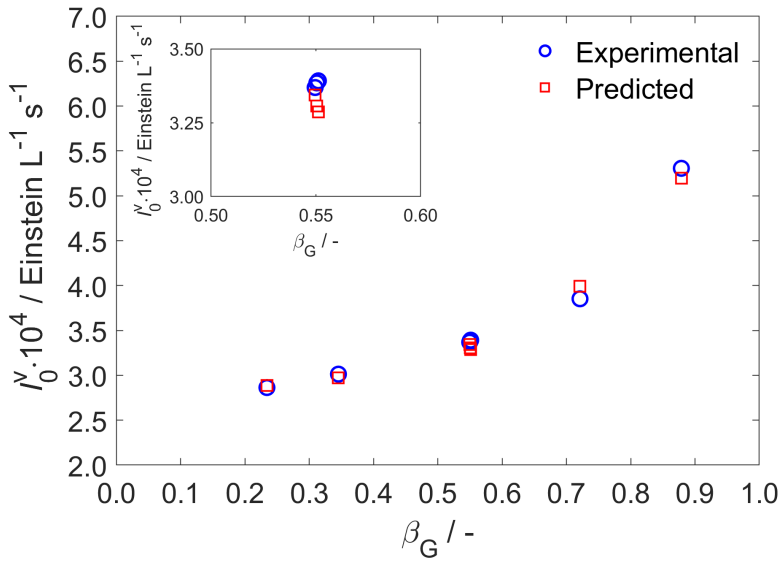

Figure 13. Comparison between the experimental and predicted photon flux per liquid volume, I_0^V, in two-phase flow at a total flow rate of 1.3 mL min^{-1}. In addition, the photon flux per liquid volumes, I_0^V, are shown for β_G = 0.55 at the total flow rates of 0.82 mL min^{-1} and 0.56 mL min^{-1}.

Starting from our model, we can propose an additional optimization strategy which involves a rational design of the Taylor flow characteristics (i.e. bubble and slug lengths, film thickness) by finding the optimal liquid volume in the highly irradiated region of the film and in the darker region of the bulk liquid.

Prediction of the optical pathlength

As previously mentioned the optical pathlength decreased with the gas fraction, β_G. If this variation can be predicted, no actinometric measurements are required when working at a different gas content. By plotting the product $(1-\beta_G)l_{reactor}$ in function of the gas fraction, β_G, a linear dependence was obtained, as illustrated in Figure 14. The intercept value was set to the optical pathlength in single-phase flow of l_{SP}= 0.797 mm. It is observed that the slope can be defined as the sum between the single-phase optical pathlength, l_{SP}, and an empirical coefficient f equal to 0.026 mm.

$$\underbrace{(1-\beta_G)l_{reactor}}_{y} = \underbrace{-(l_{SP}+f)}_{slope}\underbrace{\beta_G}_{x} + \underbrace{l_{SP}}_{intercept} \qquad (14)$$

Equation (14) can be rewritten in a simpler form as follows:

$$l_{reactor} = \frac{l_{SP}\left(1-\left(1+\frac{f}{l_{SP}}\right)\beta_G\right)}{1-\beta_G} \qquad (15)$$

While f depends on the geometry of the reactor, the optical pathlength in different reactors can be compared by the dimensionless ratio $\frac{f}{l_{SP}}$. In this study, it was found that $\frac{f}{l_{SP}}$ is equal to 0.033.

The optical pathlength in two-phase flow was recalculated using equation (15) for f = 0.026 mm, and the results are illustrated in Figure 15. As it can be observed, the correlation predicts well the optical pathlength in gas-liquid flow, as the largest deviation between predicted and experimental values was around 8.4%

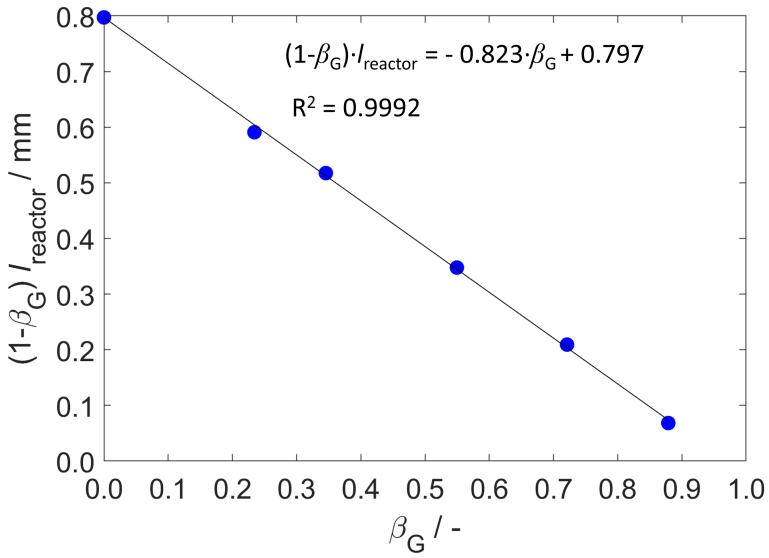

Figure 14. Correlation between the optical pathlength, $l_{reactor}$, and the gas fraction, β_G.

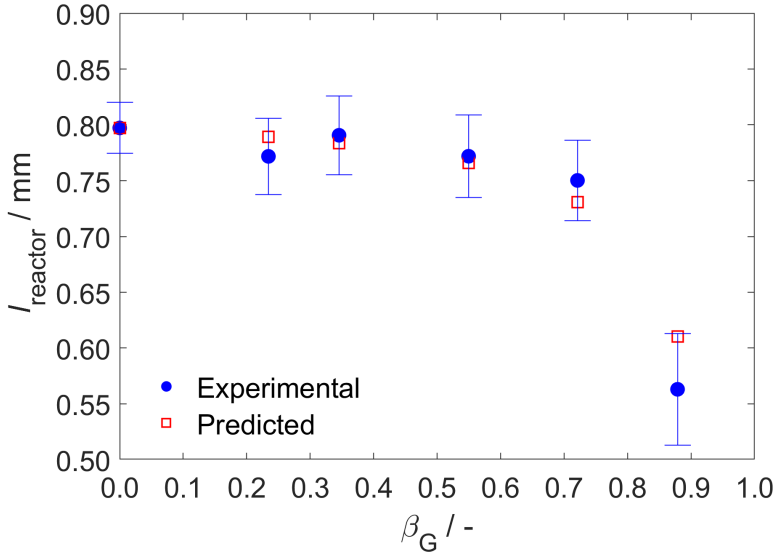

Figure 15. Comparison between the experimental and predicted optical pathlength, $l_{reactor}$, at different gas fractions, β_G.

Conclusions and outlook

The presence of a second inert phase was reported to accelerate the rate of photochemical reactions performed in Taylor flow microreactors. The higher conversions and the possibility to use more concentrated solutions in two-phase than in single-phase flow can reduce the work-up, an important advantage especially in a multi-step synthesis.[23] As introducing an inert gas could become a simple strategy to carry out very slow photochemical reactions, this work aims to provide insight in how photon transport and hydrodynamics in gas-liquid Taylor flow influence the performance of a photo microreactor.

The bubble and slug lengths, liquid residence time, photon flux per liquid volume and optical pathlength were experimentally determined at various gas fractions in a microreactor. The bubble and gas lengths correlated well with the gas fraction and were independent of the overall flow rate. The residence times obtained from RTD measurements were close to the calculated values using the plug flow assumption. The only exception was for the gas fraction equal to 0.88 which was characterized by a larger residence time than the single-phase flow at the same total flow rate. Furthermore, it was shown that the axial dispersion which was affected by the gas fraction did not affect the photoreactor performance.

The photon flux per liquid volume increased exponentially with the amount of gas in the microreactor. A 2-fold rise was observed at the highest gas fraction of 0.88 compared to single-phase flow. Consequently, we assigned

the observed large conversions to the high photon flux per liquid volume. The same flow pattern was characterized by an optical pathlength smaller with 30% in comparison with the single-phase flow.

The results of the chemical actinometric measurements were connected with the distribution of the liquid in the reactor channel, rather than the rate of liquid recirculation or light scattering. Consequently, a simple model starting from the regional liquid volumes and actinometric measurements is developed to explain and predict the rise of the photon flux per liquid volume when increasing the gas fraction. The model indicates that the photon flux per liquid volume is three times higher in the liquid film than in the bulk liquid. This difference was assigned to the light attenuation across the reactor channel. Moreover, the optical pathlength in two-phase flow was predicted using the gas fraction and the optical pathlength in single-phase flow.

This work shows that our understanding of two-phase flow photoreactors significantly improves by investigating both the photon transport and hydrodynamics. Moreover, the tools described in this study offer freedom to characterize two-phase photoreactors at a wide range of flow conditions. If the energy efficiency and throughput of a two-phase photoreactor needs to be improved, the developed model could offer guidance towards an optimal design of the flow pattern.

Further research should be realized to study the applicability of this model in the case of a photochemical reaction with a reactive gas, such as photooxidations.

Experimental Section

Chemical actinometry experiments

A mixture of the closed and open isomers of 1,2-bis(2,4-dimethyl-5-phenyl-3-thienyl)perfluorocyclopentene (TCI Chemicals) in hexane (Biosolve) is introduced in a plate microreactor (Chemtrix Inc.) using a syringe pump (Model Fusion 720, Chemyx Inc.). The nitrogen gas flow was controlled by the mass flow controller (MFC, Bronkhorst). A back pressure regulator (BPR-10, Zaiput) is placed before the gas inlet to reduce the pressure fluctuations in the reactor caused by the gas compression in the tubing connecting the MFC to the reactor inlet. The pressure drop in the gas line was measured with a pressure sensor (MPS0, Elveflow) placed before the BPR. It was also used to verify that the BPR set point was similar in all experiments. The pressure drop varied between 26 to 76 mbar for the gas flow rates ranging between 0.3 and 1.14 mL min^{-1}. The gas flow rates were measured at the outlet of the reactor using a “soap film flow meter” and it was assumed that the gas pressure in the reactor is equal to the atmospheric pressure. After setting the desired flow rates, the gas-liquid flow was allowed to stabilize for a minimum of 6 minutes (15 residence times) The microreactor is illuminated by a light source which contains 84 green LEDs (HLMP-CM3A-Z10DD, Broadcom). The current per LED was mainly 8 mA, if not otherwise specified. The mixture after reacting in the illuminated reactor channel was analyzed using a flow cell connected through optical fibers to a lamp and spectrometer (AVASPEC-ULS2048CL-EVO-RS-UA, Avantes). As the analyzed flow consists of an alternating liquid and gas phase, the absorbance measurements need to be realized with short integration time. The absorbance measurements were realized with the integration of 0.1 ms and were averaged over 300 scans. A reference and dark measurement were acquired before every experiment, by passing hexane directly through the flow cell by using a 2-way valve as illustrated in Figure 16. The Avasoft software was used to control the spectrometer during the actinometry measurements. 150 absorbance measurements were first stored to the spectrometer RAM and then were transferred to the computer. This number of measurements usually corresponds to the absorbance of 2 consecutive liquid slugs. The concentration of the DAE CF was obtained from averaging between 4 and 6 different absorbance measurements. An example of absorbance measurement and its data processing are shown in Section S1.1 in ESI.

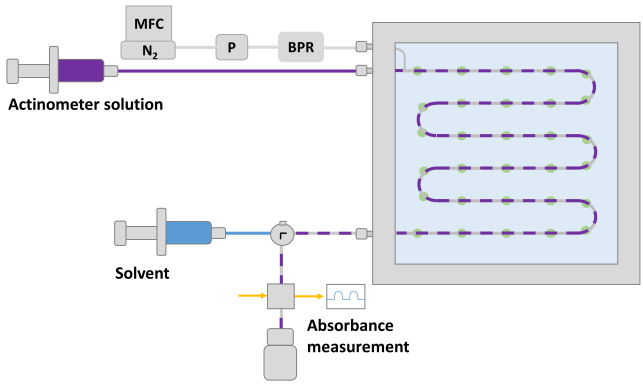

Figure 16. Experimental set-up used in the actinometric measurements. MFC is the gas mass flow controller, P is the pressure sensor, BPR is the back-pressure regulator.

Residence time distribution (RTD) experiments

The residence time of the liquid in single- and two-phase flow was determined experimentally from residence time distribution (RTD) measurements. The RTD study consists of pulse experiments which were realized using the experimental set-up illustrated in Figure 17. A solution of $1.34 \cdot 10^{-4}$ M of pyrromethene-579-8C9 (Exciton) in hexane (Biosolve) was used as a tracer. The tracer solution was injected using a 6-port valve (V-451, Upchurch Scientific) placed near to the reactor inlet. A loop which consists of a capillary tube with a volume of 4.7 µL was connected to the 6-port valve and determined the volume of the tracer injected in the reactor. The volume of the tubing and reactor holder connections was larger than the microchannel volume (0.549 mL) and influenced the RTD measurements. For this reason, the tracer concentration was measured "through the wall" using optical fibers connected to a UV-Vis spectrometer (AVASPEC-ULS2048CL-EVO-RS-UA, Avantes). The light source was the green-light LED array which was employed in the actinometric measurements. As shown in Figure 17, one optical fiber was located after the T-junction where the gas and liquid flows combine. This will be referred to as the inlet position. The second optical fiber was located near the reactor outlet and it will be referred to as the outlet position. For each flow condition, the inlet and outlet RTD measurements were repeated 4 times. The spectra acquisition was started using an in-house built trigger connected to the spectrometer. The trigger button was pushed "ON" at the moment when the valve was switched to the injection position. Because of the fast alternation of gas bubbles and liquid slugs, the integration time of the spectrometer was set to 0.5 ms, so enough data points were acquired to accurately resolve the concentration in each slug. AvasSpec-DLL interface (Avantes) was used to acquire the data provided by the spectrometer. An example of a measurement taken at the outlet position is illustrated in Figure 17. As it can be observed, the slug and bubble regions are clearly resolved.

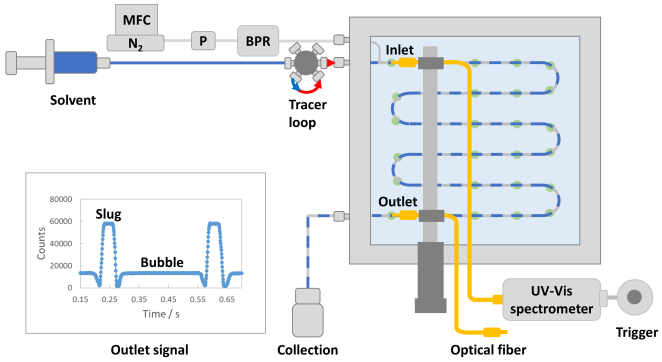

Figure 17. Schematic representation of the experimental set-up used in RTD study. The inset shows the outlet signal for β_G = 0.88 at a total flow rate of 1.3 mL min^{-1}. MFC is the mass flow controller, P is the pressure sensor, BPR is the back-pressure regulator.

Determination of the flow pattern characteristics

The characteristics of the Taylor flow were determined using flow imaging. Images of the entire reactor channel were acquired with a full-frame CMOS sensor camera (D810, Nikon) equipped with a 24-70 mm lens (AF-S NIKKOR, Nikon). The images were realized at a shutter speed of 1/3200 s and had a resolution of 7360 x 4912 $pixels^2$. The light source, a green-light LED array, was the same light source as used in the actinometric measurements. A light diffusing material was placed on the reactor glass plate on the side towards the LED array to obtain a uniform light illumination of the reactor channel. A number of three images were acquired (one image at every 20 s) for each flow condition. The obtained images were processed in Matlab to determine the bubble and slug lengths. As shown in Figure S3.1 in ESI, the microreactor channel is a serpentine with 6 straight sections. Only the slug and bubbles present in the straight sections were considered. The results from analyzing three images were averaged to obtain the average bubble length, L_b, and the average slug length, L_s. The bubble velocity was determined from videos recorded with the same camera. Videos of bubbles traveling along the entire reactor channel were recorded at 59.9 fps and with a resolution of 1920 x 1080 $pixels^2$. For each investigated two-phase flow a video of 1 min was acquired. The velocity of the bubble was determined from the time needed for the bubble to travel along each straight channel section. The travelled distance in a section was equal to 8 cm. For every flow condition, the velocity of 5 different bubbles was averaged to obtain the average bubble velocity, u_b.

References

[1] a) D. Cambié, C. Bottecchia, N. J. W. Straathof, V. Hessel, T. Noël, *Chem. Rev.* **2016**, *116*, 10276; b) C. J. Mallia, I. R. Baxendale, *Org. Process Res. Dev.* **2016**, *20*, 327.
[2] A. Gavriilidis, A. Constantinou, K. Hellgardt, K. K. Hii, G. J. Hutchings, G. L. Brett, S. Kuhn, S. P. Marsden, *React. Chem. Eng.* **2016**, *1*, 595.
[3] J. P. Knowles, L. D. Elliott, K. I. Booker-Milburn, *Beilstein J. Org. Chem.* **2012**, *8*, 2025.
[4] a) M. Nakano, T. Morimoto, J. Noguchi, H. Tanimoto, H. Mori, S.-i. Tokumoto, H. Koishi, Y. Nishiyama, K. Kakiuchi, *Bull. Chem. Soc. Jpn.* **2019**, *92*, 1467; b) K. Terao, Y. Nishiyama, K. Kakiuchi, *J. Flow Chem.* **2014**, *4*, 35.
[5] a) T. Aillet, K. Loubiere, O. Dechy-Cabaret, L. Prat, *Int. J. Chem. React. Eng.* **2014**, *12*, 1; b) T. Aillet, K. Loubière, O. Dechy-Cabaret, L. Prat, *Chem. Eng. Technol.* **2016**, *39*, 115.
[6] R. Telmesani, J. A. H. White, A. B. Beeler, *ChemPhotoChem* **2018**, *2*, 865.
[7] M. Nakano, Y. Nishiyama, H. Tanimoto, T. Morimoto, K. Kakiuchi, *Org. Process Res. Dev.* **2016**, *20*, 1626.
[8] a) R. Gupta, D. F. Fletcher, B. S. Haynes, *J. Comput. Multiph. Flows* **2010**, *2*, 1; b) P. Angeli, A. Gavriilidis, *Proc. Inst. Mech. Eng. C* **2008**, *222*, 737.
[9] a) C. Horvath, B. A. Solomon, J.-M. Engasser, *Ind. Eng. Chem. Fundam.* **1973**, *12*, 431; b) M. Abolhasani, E. Kumacheva, A. Günther, *Ind. Eng. Chem. Res.* **2015**, *54*, 9046; c) G. Bercˇicˇ, A. Pintar, *Chem. Eng. Sci.* **1997**, *52*, 3709.
[10] a) N. El Achi, Y. Bakkour, L. Chausset-Boissarie, M. Penhoat, C. Rolando, *RSC Adv.* **2017**, *7*, 29815; b) B. Wriedt, D. Kowalczyk, D. Ziegenbalg, *ChemPhotoChem* **2018**, *2*, 913; c) B. Wriedt, D. Ziegenbalg, *J. Flow Chem.* **2020**, *10*, 295.
[11] T. Tomida, M. Kubo, N. Suekuni, T. Okazaki, *Ind. Eng. Chem. Process Des. Dev.* **1986**, *25*, 203.
[12] A. Roibu, S. Fransen, M. E. Leblebici, G. Meir, T. Van Gerven, S. Kuhn, *Sci. Rep.* **2018**, *8*, 5421.
[13] a) W. Xu, Y. Su, Y. Song, M. Shang, L. Zha, Q. Lu, *Ind. Eng. Chem. Res.* **2018**, *57*, 2476; b) D. Ziegenbalg, B. Wriedt, G. Kreisel, D. Kralisch, *Chem. Eng. Technol.* **2016**, *39*, 123.
[14] A. Roibu, R. B. Morthala, M. E. Leblebici, D. Koziej, T. Van Gerven, S. Kuhn, *React. Chem. Eng.* **2018**, *3*, 849.
[15] T. Sumi, Y. Takagi, A. Yagi, M. Morimoto, M. Irie, *Chem. Commun.* **2014**, *50*, 3928.
[16] a) F. Trachsel, A. Günther, S. Khan, K. F. Jensen, *Chem. Eng. Sci.* **2005**, *60*, 5729; b) M. T. Kreutzer, A. Günther, K. F. Jensen, *Anal.Chem.* **2008**, *80*, 1558; c) A. Günther, S. A. Khan, M. Thalmann, F. Trachsel, K. F. Jensen, *Lab Chip* **2004**, *4*, 278.
[17] P. Zaloha, J. Kristal, V. Jiricny, N. Völkel, C. Xuereb, J. Aubin, *Chem. Eng. Sci.* **2012**, *68*, 640.
[18] a) M. Suo, P. Griffith, *J. Basic Eng.* **1964**, *86*, 576; b) M. J. F. Warnier, E. V. Rebrov, M. H. J. M. de Croon, V. Hessel, J. C. Schouten, *Chem. Eng. J.* **2008**, *135*, S153.
[19] a) C. Yao, Z. Dong, Y. Zhao, G. Chen, *AIChE J.* **2014**, *60*, 1132; b) V. van Steijn, M. T. Kreutzer, C. R. Kleijn, *Chem. Eng. J.* **2008**, *135*, S159.
[20] F. P. Bretherton, *J. Fluid Mech.* **1961**, *10*, 166.
[21] J. Ratulowski, H. C. Chang, *J. Fluid Mech.* **1990**, *210*, 303.
[22] J.-D. Chen, *J. Colloid Interface Sci.* **1986**, *109*, 341.
[23] M. Di Filippo, C. Bracken, M. Baumann, *Molecules* **2020**, *25*.